Measurements of the spin observables $D_{NN'}$, P, and A_y in inelastic proton scattering from ^{12}C and ^{16}O at 198 MeV

A. K. Opper,* S. W. Wissink, A. D. Bacher, J. Lisantti,† C. Olmer, R. Sawafta,‡ E. J. Stephenson, and S. P. Wells§
Indiana University Cyclotron Facility, Bloomington, Indiana 47408
(Received 13 September 2000; published 21 February 2001)

Precise values of the normal-component spin observables $D_{NN'}$, P, and A_y have been determined at an incident proton energy of 198 MeV for the $T=0$ (12.71 MeV) and $T=1$ (15.11 MeV) 1^+ states in ^{12}C for momentum transfers between 80 and 250 MeV/c, and for the $T=0$ (17.78 and 19.81 MeV) and $T=1$ (18.98 MeV) 4^- states in ^{16}O for momentum transfers of 225–400 MeV/c. The data are compared with distorted wave impulse approximation calculations in which a microscopic treatment of the nuclear medium has been used to obtain an effective nucleon-nucleon interaction. Nuclear binding and Pauli blocking effects, as well as those due to the strong scalar and vector mean field potentials that arise in covariant treatments of nuclear matter, are incorporated using a *G*-matrix approach. Our results suggest that while the isovector channel of the effective nucleon-nucleon interaction is reasonably well understood, pronounced discrepancies between theory and experiment for the isoscalar transitions point towards problems with the relative strengths of the spin-orbit and tensor components. For the ^{12}C states, these discrepancies are more difficult to interpret due to ambiguities in the nuclear structure.

DOI: 10.1103/PhysRevC.63.034614 PACS number(s): 25.40.Ep, 24.70.+s, 21.30.Fe

I. INTRODUCTION

The study of polarization transfer processes in nucleon-induced reactions has proven to be a rich source of information on both the effective (i.e., in-medium) nucleon-nucleon (NN) interaction and also on nuclear structure issues, providing much more stringent tests of current theoretical models than are possible with differential cross section ($d\sigma/d\Omega$) and analyzing power (A_y) data alone [1]. At intermediate energies, ~150–500 MeV, where the impulse approximation should serve as a valid reaction model, complete sets of $(\vec{p},\vec{p}\,')$ spin transfer observables obtained in the quasifree region have been used to separate out the spin-longitudinal and spin-transverse components of the continuum [2,3]. Concerns over the mixed isospin nature of this probe have also motivated recent studies of quasifree $(\vec{p},\vec{n})$ scattering [4,5], in which the momentum transfer q dependence of these response functions has been cleanly mapped out in the isovector channel. In a complementary way, by using inelastic nucleon scattering to induce unnatural parity, spin-flip transitions to discrete final states of well-determined structure, the spin-transfer observables that characterize this process provide information on the small and often poorly understood spin-dependent pieces of the interaction [6,7]. Moreover, by measuring these observables at intermediate energies, sensitivity to the generally weaker spin-orbit and tensor terms is further enhanced, due to the relative weakness of the usually dominant central term in this energy region.

Studies of polarization transfer in $(\vec{p},\vec{p}\,')$ reactions can therefore provide new information on the NN force inside nuclei. Because parity conservation prohibits the transfer of polarization between the normal component (directed along $\hat{N}$, perpendicular to the reaction plane) and the polarization components that lie in the reaction plane [8], there is only one normal-component polarization transfer observable, denoted here by $D_{NN'}$. Theoretical interest in measurements of $D_{NN'}$ stems from the early observation [9] that this quantity appears to be less dependent than cross sections and analyzing powers on details of the nuclear transition density used or the choice of optical distorting potential. Thus $D_{NN'}$ should serve as a sensitive and robust probe of the NN effective interaction, especially near the peak in the differential cross section [9]. These expectations are borne out in plane-wave impulse approximation (PWIA) treatments, which have shown [10] that for isovector transitions, in which the spin-orbit component should be weak, $D_{NN'}$ can be related to the ratio of the transverse and longitudinal spin components of the effective interaction. These simple relationships hold particularly well for transitions which can be characterized by a single value of LSJ transfer, such as one finds for so-called ''stretched'' states, i.e., $1p$-$1h$ excitations in which both particle and hole states have the maximum angular momentum allowed in their shells, coupled so that $J=J_{max}$, $L=J-1$, and $S=1$.

Measuring the normal component of the outgoing nucleon polarization also allows one to determine the ''induced'' polarization P, the level of polarization produced in the scattered nucleon flux for a reaction initiated with an unpolarized beam. For elastic scattering, P must equal the reaction analyzing power A_y by time-reversal invariance; thus, for inelastic scattering, the *difference* of P and A_y can probe noncollective behavior. It has been shown [11] that one can

*Present address: Department of Physics and Astronomy, Ohio University, Athens, OH 45701.
†Present address: Department of Physics and Engineering, Centenary College of Louisiana, Shreveport, LA 71134.
‡Present address: Department of Physics, North Carolina A&T State University, Greensboro, NC 27411.
§Present address: Department of Physics, Louisiana Tech University, Ruston, LA 71272.

generalize this idea and define a *spin difference* function Δ_S as

$$\Delta_S \equiv (D_{qp} + D_{pq}) + i(P - A_y), \tag{1}$$

which is identically zero for elastic nucleon scattering. (The observables D_{qp} and D_{pq} describe the transfer of polarization within the reaction plane.) In a direct-only PWIA treatment, this quantity vanishes for *inelastic* scattering as well, except for small effects related to the reaction Q value [12]. It has been shown [13], though, that Δ_S can differ significantly from zero, even within a single-scattering approximation, if nonlocal terms appear explicitly in the NN effective interaction. Such nonlocal effects can arise, for example, through explicit treatment of knock-on exchange processes, especially the important tensor exchange contributions [14]. In a relativistic formalism, in which one includes both the upper and lower (momentum-dependent) components of the bound nucleon wave functions, effective couplings between the projectile and the nuclear convection currents ($\vec{j}$) and composite spin-convention currents ($\vec{\sigma}\cdot\vec{j}$ and $\vec{\sigma}\times\vec{j}$) appear naturally [11,13,15]. Because exchange effects are generally expected to decrease in strength with increasing bombarding energy, examining the energy dependence of Δ_S should provide insight into the source and nature of these nonlocalities.

As part of a broader program at the Indiana University Cyclotron Facility (IUCF) to investigate the spin-dependent terms of the effective nucleon-nucleon interaction at intermediate energies, we have measured the normal-component polarization observables $D_{NN'}$, P, and A_y for the excitation of five unnatural-parity states in light nuclei via inelastic scattering of 198-MeV protons. The transitions chosen include the two dominant 1^+ states in ^{12}C at 12.71 MeV ($T=0$) and 15.11 MeV ($T=1$), and the three 4^- stretched states in ^{16}O at 17.78 and 19.81 MeV ($T=0$) and 18.98 MeV ($T=1$). These data, when combined with previously measured in-plane spin transfer coefficients for the same five transitions [16] provide, for the first time, several complete sets of spin transfer observables over a wide range of momentum transfer near 200 MeV. Several groups have shown [6,7] that by forming specific linear combinations of these observables, one can gain increased sensitivity to individual terms in the effective NN interaction [17].

We now briefly discuss some earlier work involving these particular nuclear transitions. The strong isoscalar and isovector 1^+ states in ^{12}C have been extensively studied, both theoretically and experimentally, primarily as tests of our understanding of the in-medium NN interaction at low momentum transfer. Early measurements at 397 MeV [9] of $D_{NN'}$ for the isovector 1^+ transition indicated that the tensor amplitudes were not well understood at that time for momentum transfers as low as 150 MeV/c. More severe discrepancies, though, were found between data and distorted wave impulse approximation (DWIA) calculations of $D_{NN'}$ for the isoscalar 1^+ transition. These latter differences were thought to be due either to uncertainties in the nuclear structure of this state, or to problems with the relative strengths of the spin-orbit and tensor interactions in the isoscalar channel [9].

The first complete sets of $(\vec{p},\vec{p}\,')$ observables for these states were obtained at Los Alamos at 500 MeV [18]. These data have since been remeasured at the same energy with higher precision [19], though typical errors (statistical plus systematic) remain greater than 0.05 at the most forward angles and increase rapidly with scattering angle. The authors concluded that no single calculation could provide a good description of all observables [19] and most of the problems alluded to in the previous paragraph were again found to plague interpretation. Within their uncertainties, however, the authors were able to extract spin response functions beyond those accessible via electron scattering.

More recent studies at IUCF [20] used simultaneous measurements of $(\vec{p},\vec{p}\,')$ and $(\vec{p},p'\gamma)$ observables to examine the isovector 1^+ state in ^{12}C in great detail at 200 MeV. The large number of observables obtained (16), and the statistical precision of the data, allowed for a complete determination of the scattering amplitude for this transition, in an essentially model-independent manner, at four values of momentum transfer. Supporting earlier suggestions by the Los Alamos group [18,19], it was found [20] that the best overall agreement with the data set was provided by calculations which used a relativistic description, but in which knock-on exchange processes had *not* been explicitly included. Despite the high quality of the data obtained, the reliance on $(\vec{p},p'\gamma)$ observables to complement the $(\vec{p},\vec{p}\,')$ information limits the number of nuclear transitions which can be probed efficiently using this technique.

Several earlier studies focused on only the normal-component observables, at a variety of energies. Measurements of $(P-A_y)$ at 150 MeV [21] showed surprisingly large deviations from zero for both the isoscalar and isovector 1^+ states in ^{12}C. Qualitatively similar results were reported for $(P-A_y)$ at 200 MeV for the $T=1$ state in Ref. [20], in which two different measurement techniques were used to determine the same observable. These results are to be contrasted with the much smaller values of $(P-A_y)$ obtained in studies at 400 MeV [22] and 500 MeV [19] for both the $T=0$ and $T=1$ 1^+ states. This decrease in magnitude with increasing beam energy is consistent with the assumption that $(P-A_y)$ is driven primarily by tensor exchange contributions, which are expected to become less important at higher energy. Further studies of the energy dependence of this observable may provide insight into the source of the nonlocalities that are present in the interaction.

The three strong stretched 4^- states in ^{16}O have also been the subject of previous work. For all three states, the nuclear structure is expected to be dominated by the promotion of a single nucleon from the $p_{3/2}$ to the $d_{5/2}$ level, with particle and hole coupled to the maximum allowable total angular momentum ($LSJ=314$). Because only a single value of angular momentum ($L=J-1$) is transferred to the target, in a simple shell model picture the longitudinal and transverse transition densities become proportional to one another [23]. More detailed information on the structure of the individual states has come from comparative analyses of (e,e') [24] and (π,π') scattering [25,26]. Based on the relative strengths observed in π^+ and π^- scattering studies, the isos-

pin admixtures have been determined, establishing the 18.98 MeV state as being essentially pure $T=1$, and the 17.78 and 19.81 MeV states as predominately $T=0$, but with small isovector components of comparable size but opposite signs.

Because the nuclear structure of these stretched states is reasonably well determined, studies of their excitation can provide some of the most stringent tests of the validity of models for the effective *NN* interaction [17]. The high spin of these states also results in (p,p') cross sections that tend to peak at reasonably large angles, thus allowing for investigation at high momentum transfer with high statistical precision. For the isovector transitions, in which the spin-orbit force is relatively weak, this may provide fairly direct information on the tensor terms; for the isoscalar states, on the other hand, both tensor and spin-orbit components will be present, though the relative strengths of these terms is poorly determined, and varies widely among competing interaction models.

Despite these important features, the number of $(\vec{p},\vec{p}\,')$ spin observables (other than A_y) that have been measured for the 4^- states in ^{16}O is surprisingly small. Complementing the normal-component observables studied in this work are the in-plane polarization transfer coefficients at 198 MeV measured by Olmer *et al.* [16]. A complete set of observables was measured at 350 MeV by a group at TRIUMF [27]. Other related work includes the measurement of a complete set of $(\vec{p},\vec{p}\,')$ spin transfer observables for the strong 5^- and 6^- (stretched) states in ^{28}Si at 500 MeV [28], and several recent 198 MeV $(\vec{p},\vec{p}\,')$ studies at IUCF on stretched states in ^{10}B [29] and ^{28}Si [30,17].

This paper is organized as follows. In Sec. II, we present the theoretical background and formalism used for analysis of the data, in order to show more explicitly the relationships between experimental observables and results derived from model calculations. Descriptions of the detectors employed and other technical details concerning the apparatus are provided in Sec. III, along with information on the conditions present and procedures followed during data acquisition. In Sec. IV we discuss data reduction and analysis issues, concentrating on polarimetry, yield extraction methods (which differed for the two nuclei), and conversion of yields to final observables. Section V contains brief descriptions of the model calculations, and compares the predictions of these models to our data. Our most significant results and conclusions are summarized in Sec. VI.

II. THEORETICAL BACKGROUND

In order to illustrate the physics content of the spin transfer coefficients (the D_{ij}'s) and to make more explicit several of the assumptions that will be used in the discussion of our results, it is useful to examine the precise relationship between the nucleon-nucleus (*NA*) scattering observables and those that parameterize nucleon-nucleon (*NN*) scattering. Adopting the conventions of Kerman, McManus, and Thaler (KMT) [31], the most general form allowed by parity and time reversal invariance for the free *NN* scattering amplitude in a nonrelativistic framework is given by [32]

$$M_t(q)=A+B\sigma_{\hat{n}}^t\sigma_{\hat{n}}+C(\sigma_{\hat{n}}^t+\sigma_{\hat{n}})+E\sigma_{\hat{q}}^t\sigma_{\hat{q}}+F\sigma_{\hat{p}}^t\sigma_{\hat{p}} \quad (2)$$

with

$$\vec{q}=\vec{k}'-\vec{k}, \quad \vec{n}=\vec{k}\times\vec{k}', \quad \hat{p}=\hat{q}\times\hat{n}, \quad (3)$$

where $\vec{k}$ ($\vec{k}'$) is the incident (scattered) proton momentum, the Pauli spin operators σ that are t superscripted (non-superscripted) are for the target (projectile) nucleon, and the complex amplitudes *A*, *B*, *C*, *E*, and *F* are assumed to exhibit an isospin dependence of the form $A=A_1+A_2(\vec{\tau}^{\,t}\cdot\vec{\tau})$, etc.

The plane wave impulse approximation allows us to express the *NA* scattering amplitude $\overline{M}(q)$ in terms of the *NN* amplitudes defined above. For a 0^+ target excited via proton inelastic scattering to a state J^π, this takes the form

$$\overline{M}(q)=\langle J\mu|\sum_t M_t(q)e^{-i\vec{q}\cdot\vec{r}_t}|0\rangle, \quad (4)$$

where M_t is now to be interpreted as the amplitude for scattering of the incident proton from the tth target nucleon. We can *define* the polarization transfer coefficients D_{ij} in terms of the *NA* scattering amplitude and the nucleon spins, using the conventions of Wolfenstein [32]:

$$\frac{d\sigma}{d\Omega}D_{ij}\equiv\frac{1}{2}\mathrm{Tr}[\overline{M}\,\sigma_i\,\overline{M}^\dagger\,\sigma_j], \quad (5)$$

where σ_i (σ_j) is the Pauli spin matrix for the ith (jth) component of the incident (scattered) nucleon polarization, and

$$\frac{d\sigma}{d\Omega}\equiv\frac{1}{2}\mathrm{Tr}[\overline{M}\,\overline{M}^\dagger] \quad (6)$$

is the usual unpolarized differential cross section. Written in this form, it is apparent that values for all of the reaction observables can be easily generated, given a model calculation for $\overline{M}$. We also note that by explicitly separating the target nucleon spin dependence in M_t, the transition amplitude can be factored into interaction-dependent and nuclear-structure-dependent components.

We can see from the above equations that the polarization transfer observable D_{ij} relates the ith component of the initial (incident) proton polarization to the jth component of the final (outgoing) proton polarization. Because i and j each run over four possible values, corresponding to the identity matrix and the three Pauli spin-matrices, potentially 16 independent spin observables would need to be determined to characterize a $0^+\rightarrow J^\pi$ transition excited via either nucleon inelastic scattering or nucleon charge exchange. Ohlsen has shown [8], in an intuitive manner, that invoking parity conservation and time reversal reduces the number of nonzero observables to eight, since interactions that respect these symmetries cannot mix polarization components normal to the scattering plane with those that lie in the plane. The relationship between the polarization components of the incident and outgoing nucleon may therefore be expressed in the following general matrix form:

$$\frac{d\sigma_p}{d\Omega}\begin{bmatrix}1\\ p_n'\\ p_p'\\ p_q'\end{bmatrix}=\frac{d\sigma}{d\Omega}\begin{bmatrix}1 & D_{n0} & 0 & 0\\ D_{0n} & D_{nn} & 0 & 0\\ 0 & 0 & D_{pp} & D_{qp}\\ 0 & 0 & D_{pq} & D_{qq}\end{bmatrix}\begin{bmatrix}1\\ p_n\\ p_p\\ p_q\end{bmatrix} \tag{7}$$

where $d\sigma_p/d\Omega$ is the polarized cross section,

$$\frac{d\sigma_p}{d\Omega}=\frac{d\sigma}{d\Omega}(1+D_{n0}p_n). \tag{8}$$

The observable D_{0n}, which characterizes a reaction in which the incident beam is unpolarized and the normal component of the scattered beam is measured, is equivalent to the induced polarization P discussed previously, while D_{n0} is the scattered yield asymmetry due to a normally polarized incident beam, i.e., the reaction analyzing power A_y. In this work, all spin observables will be described in the laboratory coordinate frame, in which the polarization components of the incident proton are measured in the unprimed coordinate system $(\hat{N},\hat{L},\hat{S})\equiv(\hat{n},\hat{k},\hat{n}\times\hat{k})$, while those of the scattered proton are measured in the primed coordinate system $(\hat{N}',\hat{L}',\hat{S}')\equiv(\hat{n},\hat{k}',\hat{n}\times\hat{k}')$.

III. EXPERIMENTAL DETAILS

The measurements described in this paper were carried out at the Indiana University Cyclotron Facility (IUCF) using the high-resolution K600 spectrometer [33] and its associated focal plane polarimeter (FPP) [34]. From the preceding discussion, it is clear that in order to determine the complete set of normal-component polarization observables ($D_{NN'}$, P, and A_y), one must know the component of the proton polarization vector perpendicular to the scattering plane immediately before and after the scattering (p_N and $p_{N'}$, respectively). For this work, information on the incident beam spin was obtained from a low-energy polarimeter mounted between the injector and main stage cyclotrons, while the FPP, mounted just downstream of the K600 focal plane, provided information on the outgoing proton polarization.

The 198 MeV polarized proton beam was produced using an atomic beam polarized ion source [35]. In this type of ion source, the beam polarization can be ''flipped'' from one spin state to another (e.g., from ''up'' to ''down'' in the laboratory frame) via rf transitions, without significantly affecting either the intensity or trajectory of the transported beam. During actual data acquisition, the beam polarization direction was reversed every 30 seconds to minimize sensitivity to various instrumental asymmetries. The magnitude of the incident beam polarization for each spin state was measured approximately once every 24 h with a low energy polarimeter [36] that used $p+{}^4$He elastic scattering as the analyzing reaction. Periodically, additional polarimeter measurements were taken with the atomic beam valve on the ion source closed; in this way, an unpolarized beam (albeit, one of low intensity) was incident on the polarimeter target,

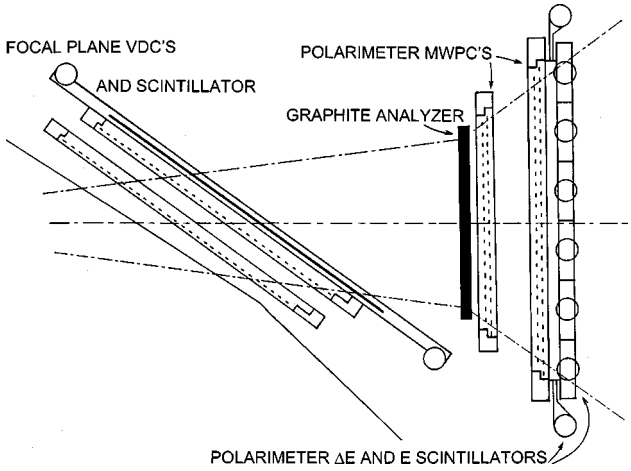

FIG. 1. Top view of the IUCF K600 focal plane and focal plane polarimeter detectors.

and any left-right asymmetry observed could be used to correct for instrumental or geometric effects in the device. Over the running period of this experiment (approximately two weeks), the primary proton beam polarization averaged 0.76 for each spin state, with typical magnitude differences of less than 0.01 observed between the two spin states. This difference is comparable to the error achieved in each measurement, due primarily to uncertainties in elastic scattering yield extraction. In our final determination of the spin observables, we therefore used a simple average of the spin-up and spin-down polarization magnitudes, after each had been corrected for polarimeter false asymmetries. Long-term drifts in the beam polarization, i.e., over a 24 h period, never exceeded 0.015.

In order to ensure that most sources of systematic error were small and under control, a number of consistency checks were included in our data collection and analysis procedures. A detailed description of the K600/FPP facility and its calibration results have been provided elsewhere [34], and will be summarized only briefly here.

Charged particles emitted in the primary scattering reaction are momentum analyzed as they pass through the dipole fields of the horizontal-bend-plane K600 spectrometer. Coils internal to the spectrometer provide kinematic (quadrapole) and hexapole aberration corrections. The scattered particles then pass through the focal plane and FPP detector stack, shown schematically in top view in Fig. 1. The focal plane detection system consists of two parallel vertical drift chambers (VDC's) followed by a single thin plastic scintillator (S1 in Fig. 1). The VDC's provide high resolution position and angle information on the proton trajectory, while the scintillator data are used for particle identification and fast timing. The polarimeter, mounted just downstream of the focal plane stack and oriented approximately perpendicular to the central momentum ray, consists of a thick (5 cm) graphite block, which functions as the polarization analyzer, followed by two sets of paired $x-y$ multiwire proportional chambers (MWPC's), backed by two planes of plastic scintillator. Hit pattern data from the MWPC's are used to determine the proton's trajectory upon leaving the analyzer; in

conjunction with the focal plane information, this establishes the true scattering angle in the analyzer and verifies that the (secondary) event origin lies within this block. The final two scintillator planes, 0.64 and 7.62 cm thick, confirm the particle identification information, and also provide a measure of the inelasticity of the second (analyzer) scattering reaction.

The trigger logic and readout electronics scheme used were relatively simple. All modules were gated or strobed whenever the focal plane and FPP scintillators both fired in coincidence with at least one wire hit in each of the focal plane VDC's. For this experiment, we also incorporated a second level trigger, a decision based on the encoded data words available from the FPP MWPC's via the LeCroy [37] PCOS III system. Feeding this information into a fast memory look-up unit for bit-pattern recognition enabled us to perform rapid (<500 ns) hardware rejection of events in which the detected particle underwent no significant scattering (less than $\sim 3°$) in the graphite analyzer. By eliminating these ''straight through'' events, the effective data acquisition rate could be increased by approximately a factor of 5. For this work, we also accepted a prescaled fraction (typically 1 in 10) of all valid focal plane events, independent of the second level trigger requirement, to allow for absolute cross section and analyzing power determinations, as well as calibration information on the polarimeter geometry.

Because the K600 spectrometer has a horizontal bend plane, the longitudinal and sideways (''in-plane'') components of the scattered beam polarization are mixed in passing through the dipole fields, but the vertical component, normal to the scattering plane, is unaffected. Thus a measurement of the left/right asymmetry observed in scattering from the carbon block, combined with knowledge of the effective analyzing power of the FPP (A_{FPP}), allows for direct extraction of the normal component of the scattered beam polarization. The value of A_{FPP}, determined in separate calibration studies [34], is dependent on the kinetic energy of the proton being analyzed. For the measurements described here, A_{FPP} decreased smoothly from 0.471 down to 0.415 as the proton energy decreased from 187 to 175 MeV. The corresponding efficiency of the FPP (η_{FPP}) over the same energy interval ranged between 1.96 and 2.27%, showing a slight rise with decreasing proton energy. These values for A_{FPP} and η_{FPP} are in reasonable agreement with those obtained in studies conducted at other facilities using similar instruments [38,39].

The ^{12}C data taken at angles greater than 15.5° were obtained using a thin (10.8 mg/cm^2) natural carbon target in order to achieve high resolution, typically 35 keV full width at half maximum (FWHM). In spite of the thinness of this target, a reasonable count rate could be maintained by using beam currents as high as 100 nA. At these angles, it was possible to collect the unscattered beam in a well-shielded beam dump, located approximately 8 m beyond the scattering chamber. For scattering angles forward of 15.5°, however, it was necessary to stop the beam in an electrically isolated Faraday cup mounted inside the scattering chamber, which precluded extensive shielding. Under these conditions, increased room background from the Faraday cup led to an increase in the leakage currents drawn by the MWPC's, and incident beam currents of no more than ~ 6 nA could be tolerated. To compensate, a thicker (22.0 mg/cm^2) natural carbon target was used at the smaller angles, which degraded the energy resolution in the spectrometer to approximately 60 keV.

In the oxygen work, an 11.2 mg/cm^2 target of H_3BO_3 was used, for an effective ^{16}O thickness of 8.81 mg/cm^2. The boron was isotopically enriched in ^{10}B, since the ^{11}B(p,p') spectrum contains additional peaks in the excitation energy region of interest. The target had 260 μg/cm^2 gold leaf attached to the front and back surfaces to aid in heat dissipation and to inhibit evaporation under beam heating. Despite the intrinsic high resolution capabilities of the K600 spectrometer system, the energy resolution of the states of interest in ^{16}O was typically limited to ~ 70 keV FWHM, due predominantly to nonuniformity in the thickness of the target material.

The entrance aperture to the spectrometer was defined by a rounded slot, 1.27 cm wide and 2.54 cm high, milled through a piece of thick (~ 1.3 cm) brass positioned 71.3 cm from the center of the scattering chamber. This corresponds to a horizontal acceptance of approximately 1° and a vertical acceptance of about 2°, well within the width and height limitations set by the vacuum box within the K600 dipoles. With this aperture, the solid angle subtended was 0.57 msr.

For these studies, the K600 focal plane detector system was configured in its ''medium-dispersion'' mode, and had a maximum momentum bite of about 9%. This translates to an energy bite of roughly 36 MeV for proton energies near 200 MeV. In the kinematic regimes and under the running conditions typically encountered in this work, use of the full focal plane would have resulted in at least 60% of the momentum acceptance (and often 75% of the total event rate) lying outside the regions of excitation energy that constituted the primary focus of this experiment. During production running therefore two techniques were used to eliminate these events from the data stream. Protons on the high momentum side, such as those that scattered elastically in the primary target, were stopped on a thick copper block mounted on a movable track inside the K600 vacuum box just upstream of the focal plane detector stack. To exclude the lower momentum (higher excitation energy) contributions, preamplifier cards on the focal plane VDC's were selectively disabled. In this way, the high flux of elastically scattered protons did not produce any first-level triggers at all, while events that fell in regions of high excitation were vetoed out at a second level in hardware. As a result, an energy acceptance of ~ 14 MeV was used for most of the work described here.

IV. DATA ANALYSIS

A. Overview of method

The observed differences in yield for protons that scatter left or right in the carbon analyzer, for incident beam polarizations oriented ''up'' or ''down,'' can be related to the spin observables $D_{NN'}$, P, and A_y that characterize the primary scattering reaction. These relationships will be derived more

explicitly below, after a brief discussion of the conditions imposed in software to identify valid spectrometer and polarimeter events.

To be considered a useful event, the detected particle must first pass a $\Delta E-\Delta E$ pulse-height correlation requirement, formed between the thin focal plane scintillator and the ΔE FPP scintillator (see Fig. 1). This ensures its identification as a proton of approximately the desired kinetic energy. (The spectrometer acceptance already provides a fairly stringent ''hardware'' momentum cut.) The VDC information, consisting typically of three or four consecutive wire hits per chamber, plus associated drift time information, is then thoroughly checked for internal consistency, and precise values for the trajectory parameters (position and angle) through the detector stack are determined. At this point, the horizontal position at which the proton crossed the focal plane, which is closely correlated with the scattered proton momentum, can be calculated, and the process is considered a valid spectrometer event. The distribution of yield across the focal plane can also be sorted by the spin state of the incident proton beam, and cross sections and analyzing powers for the discrete states or excitation energy regions of interest can then be deduced by the usual methods.

If the focal plane polarimeter is in use, valid spectrometer events are subjected to a second set of software tests. After checking the integrity of the FPP MWPC event structure, the trajectory of the proton *after exiting the graphite analyzer* is determined. Combined with the focal plane information, a secondary scattering vertex can be located. The analysis program requires that this vertex (calculated separately in the x and y directions) lies within the physical boundaries of the analyzer, after allowing for uncertainties due to the finite angular resolution of the wire chambers and for multiple scattering effects on the proton's trajectory as it passes through the thick carbon analyzer. The FPP scintillator pulse-height data are then converted to absolute energy losses and corrected for geometric effects (based on the MWPC information), and tighter particle identification cuts are applied. Additional internal consistency checks were also used in this work to recover most of the events in which multiple hits were recorded in one or more of the FPP wire chambers. By eliminating spurious or nonphysical trajectories, it was usually possible to reduce the event information to a single allowed proton track, and then subject the data to the same sequence of energy and angle cuts as the single-hit events.

For our final data sample in these studies, we kept only those events in which the x (horizontal) projection of the analyzer scattering angle fell between 5.5 and 23.2°, and for which the energy deposition measured in the 7.62-cm-thick FPP scintillator was within ~6 MeV of the energy deposition one would expect if the proton had undergone a single elastic scattering on a ^{12}C nucleus within the analyzer. (A similar, but less stringent, requirement was also imposed on the measured FPP ΔE information.) These two criteria, which respectively select a particular range of scattering angles and discriminate against inelastic scattering processes, were chosen empirically to maximize the figure-of-merit of the FPP, while maintaining a high effective analyzing power for the device.

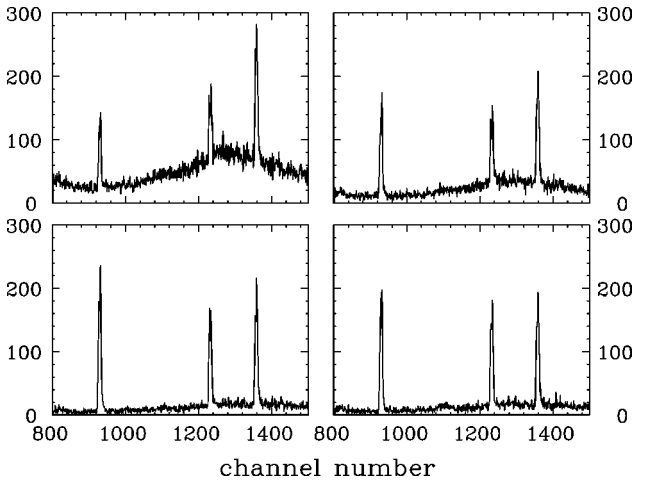

FIG. 2. Focal plane spectra of 198-MeV protons scattering from ^{12}C, sorted by scattering angle in the analyzer and incident proton spin state. The left (right) pair represent scattering to the left (right) and the top (bottom) are for incident beam spin up (down).

Events which satisfied the above conditions (''valid FPP events'') were then sorted by scattering direction in the analyzer (left or right) and incident spin state (up or down), and histograms of yield along the focal plane were generated. An illustrative example is presented in Fig. 2, for scattering of 198 MeV protons from ^{12}C at 16°. The top (bottom) pair of spectra are for incident beam spin up (down), and the left (right) pair represent scattering to the left (right), as defined by the Madison convention. The narrow peaks near channels 4700, 5300, and 5600 correspond to excitation of the 12.71, 15.11, and 16.11 MeV states in ^{12}C, respectively.

The final step in the data analysis involves extraction of the relative yields for the transitions of interest from these four ''spin-state sorted'' spectra, followed by calculation of the asymmetries associated with each polarization observable. The procedures used for yield extraction are quite complex, and differed for the ^{12}C and ^{16}O spectra; these will be described in some detail in the following subsections. For now, we note that once the spin-sorted proton yields have been obtained, it is quite straightforward to derive expressions for the normal-component spin observables in terms of these yields. Consider the number of valid FPP events in which the proton is scattered to a given side (left or right) for a given incident spin state. We have

$$N=\eta_{FPP}\,I\,(1+p_{N'}\,A_{FPP}), \tag{9}$$

where N is the yield measured in the FPP, η_{FPP} is the FPP detection efficiency, I is the flux of scattered protons (from the primary reaction) for the transition of interest, $p_{N'}$ is the vertical polarization of this scattered flux, and A_{FPP} is the effective analyzing power of the polarimeter. Looking at these factors individually, we note that the FPP efficiency can be expressed somewhat schematically as

$$\eta_{FPP}=\left\langle \frac{d\sigma}{d\Omega}\cdot t\cdot \Delta\Omega \right\rangle_{FPP}, \tag{10}$$

in which $d\sigma/d\Omega$ is (predominantly) the elastic scattering cross section for protons on ^{12}C, t is the analyzer thickness, and $\Delta\Omega$ is the solid angle acceptance of the FPP. Note that these parameters must be averaged over a range of incident energies, excitation energies, and scattering angles, and therefore depend not only on the particular hardware configuration used, but also on the choice of software conditions imposed. Thus ''effective'' values must be determined empirically through precise calibration procedures [34].

From Eq. (8), we see that the scattered flux I is related to the flux one would measure with an unpolarized incident beam I_0 plus a term dependent on the normal component of the incident beam polarization,

$$I=I_0(1+p_N A_y). \tag{11}$$

The normal component of the scattered beam polarization is shown in Eq. (7) to be given by

$$p_{N'}=\frac{P+p_N D_{NN'}}{1+p_N A_y}. \tag{12}$$

We now combine Eqs. (9)–(12) to obtain our primary result:

$$N=\eta_{FPP}\, I_0\,(1+p_N A_y+PA_{FPP}+p_N D_{NN'}A_{FPP}). \tag{13}$$

This equation shows explicitly the relationship between the measured FPP yield (N) and the spin observables of interest for the primary reaction (A_y, P, and $D_{NN'}$). This relationship is expressed in terms of the FPP performance parameters (η_{FPP} and A_{FPP}), the incident proton beam polarization (p_N), and the scattered proton flux (I_0); this last quantity can be measured directly using the spin-sorted focal plane yields (see below), and is a function of the (primary) reaction cross section, integrated charge, spectrometer solid angle, and primary target thickness.

The FPP yield N can be measured for protons scattered in the analyzer to the left [Eq. (11)] and to the right (A_{FPP} flips sign), using incident proton beams with spin up ($p_N>0$) or spin down ($p_N<0$). If we assume that the incident beam polarization ''flips'' exactly, i.e., that $|p_{N\uparrow}|=|p_{N\downarrow}|\equiv p_N$, and also that I_0 is the same for each spin state, then these four FPP yields can be combined to produce the following simple relationships between the spin observables of interest and the measured quantities:

$$A_y=\frac{1}{p_N}(L_\uparrow+R_\uparrow-L_\downarrow-R_\downarrow)/S, \tag{14a}$$

$$P=\frac{1}{A_{FPP}}(L_\uparrow-R_\uparrow+L_\downarrow-R_\downarrow)/S, \tag{14b}$$

$$D_{NN'}=\frac{1}{p_N\cdot A_{FPP}}(L_\uparrow-R_\uparrow-L_\downarrow+R_\downarrow)/S, \tag{14c}$$

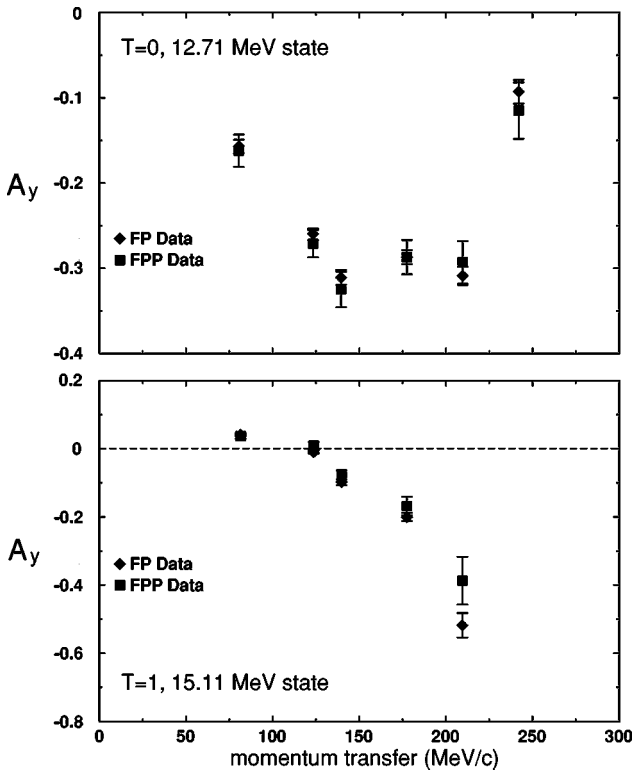

FIG. 3. Comparison of values for A_y deduced from the prescaled focal plane data (diamonds) and the focal plane polarimeter data (squares) for the 1^+ states in ^{12}C.

where S is the sum of all four yields, $S\equiv L_\uparrow+R_\uparrow+L_\downarrow+R_\downarrow$, and where $L_\uparrow$ represents the number of protons scattered to the left for a spin-up incident beam, etc.

In this work, Eqs. (14) were used to determine the spin observables, with small modifications applied to correct for deviations from the two assumptions made above. First, the raw FPP yields were normalized to account for spin-dependent differences in I_0 due primarily to electronic and computer livetime, wire chamber inefficiencies, and integrated primary beam flux. Second, we note that any difference in the magnitudes of the incident beam polarizations for the two spin states requires that the above equations for A_y and $D_{NN'}$ be modified (to first order) by including an overall multiplicative factor

$$\beta_{cor}=[1-\Delta p_N A_y]^{-1}, \tag{15}$$

where $\Delta p_N\equiv\frac{1}{2}(|p_{N\uparrow}|-|p_{N\downarrow}|)$. (The corresponding correction for P is only slightly more complicated.) Given the typical differences between the up and down polarization magnitudes, as measured with the low energy polarimeter ($\leqslant 0.01$; see Sec. III), and the small size of A_y for most of these transitions, this correction would in all cases amount to less than a 0.5% renormalization of the observables. This factor was therefore not applied to the data, as the fractional uncertainty in the beam polarization and the FPP analyzing power are each several times larger than this, as are the statistical errors for most observables.

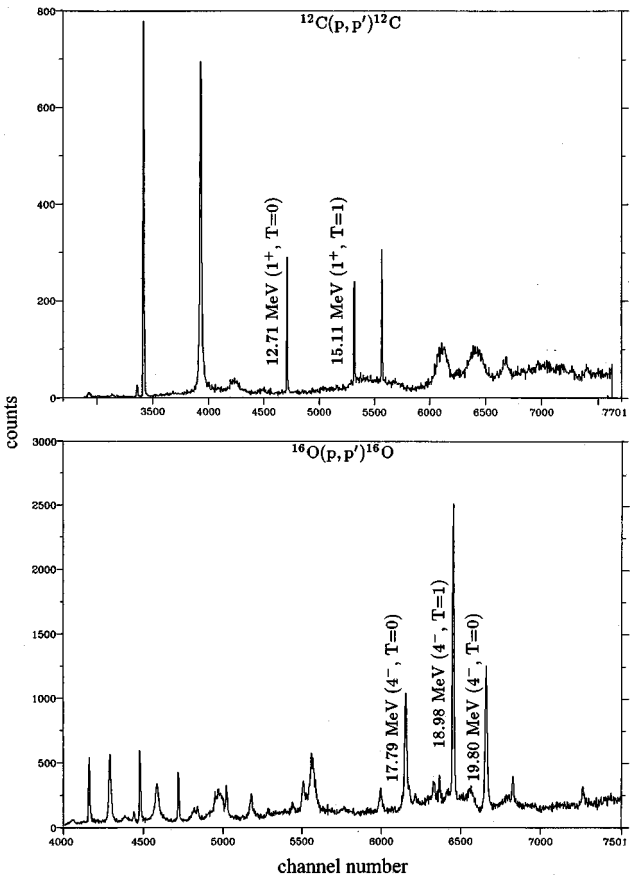

FIG. 4. Typical raw excitation spectra for 198-MeV protons scattering from ^{12}C (top) and ^{16}O (bottom).

For completeness, it is useful to note that, just as the form of the FPP yields as described in Eq. (13) leads to the spin-transfer observables via Eqs. (14), the form of the spin-dependent focal plane yield, described in Eq. (11), leads to two additional equations:

$$I_0=\frac{1}{2}(I_\uparrow+I_\downarrow), \tag{16a}$$

$$A_y=\frac{1}{p_N}(I_\uparrow-I_\downarrow)/I_0, \tag{16b}$$

where $I_\uparrow$ and $I_\downarrow$ represent the (normalized) yields measured in the spectrometer focal plane for spin-up and spin-down incident proton beams, respectively. From these equations, we see that the analyzing power for the primary reaction, A_y, can be calculated using only the spin-sorted spectrometer events (independent of the FPP) *or* from analysis of just the FPP yields [using Eq. (14a)] As a consistency check, we can compare the values of A_y deduced from these two techniques which involve almost mutually exclusive data sets, and which are sensitive to different forms of systematic error. One set of comparisons, for the two 1^+ states in ^{12}C, is presented in Fig. 3. The results are in very good agreement with each other, and indicate no statistically significant difference between the results of the focal plane and FPP analyses for this observable.

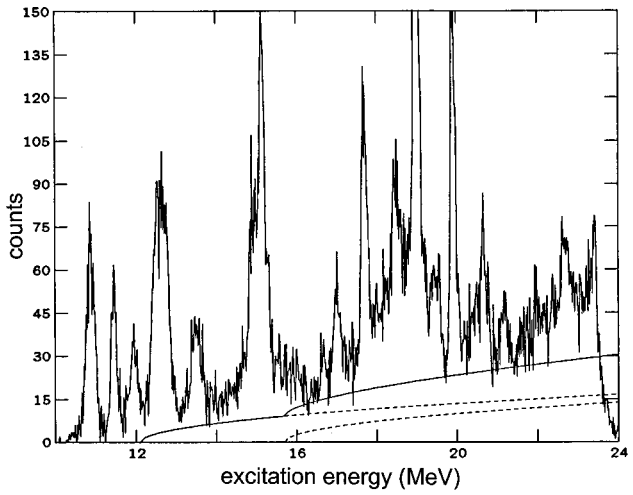

FIG. 5. Expanded oxygen spectrum with ''background'' given by Eq. (18). The solid curve under the data represents the smooth background assumed to be due to quasielastic scattering.

For reference, in Fig. 4 we present typical spectra for 198-MeV proton scattering from ^{12}C and ^{16}O over the excitation energy regions studied in this work. While these spectra display the high resolution attainable with the K600, they also indicate the significant amounts of background that underlie the peaks of interest. In general, this ''background'' yield may contain contributions from the tails of adjacent or very broad peaks and from continuum (knockout) processes, plus slit-edge scattering from the entrance collimator or spectrometer vacuum cans, and even time-uncorrelated room background events. The yields from all of these processes will, in general, vary with scattering angle and may be spin dependent, and thus must be accounted for before one can determine the correct peak area for the transitions of interest for each spin state. It is also clear that these background components enter differently in the ^{12}C and ^{16}O spectra. Different yield extraction methods were therefore developed for each nucleus, and will be described next.

B. Yield extraction for ^{12}C

The intrinsic widths of the unnatural-parity 1^+ states in ^{12}C at 12.71 and 15.11 MeV ($\Gamma=0.018$ and 0.042 keV, respectively) [40] are very much narrower than the widths attained experimentally ($\sim$35 keV), the latter being determined by resolution limits of the beam and spectrometer system. In this region of excitation energy, however, most of the peaks observed result from natural parity transitions, which often have intrinsic widths significantly greater than 35 keV. Moreover, many of these natural parity transitions, and especially those with large cross sections, tend to be characterized by spin observables that are quite similar from state to state, and resemble those for elastic scattering (i.e., $D_{NN'}\approx 1$, etc.). It is not unreasonable therefore to expect that from roughly 10 to 18 MeV excitation, the polarization observables for the background yields should differ considerably from those for the two states of interest, and, more importantly, will vary smoothly in energy on a scale somewhat larger than the observed widths of those states.

TABLE I. Normal-component spin observables for the 1^+, $T=0$ (12.71 MeV) state in ^{12}C.

θ_{LAB}	$\theta_{\text{c.m.}}$	q (MeV/c)	A_y	P	$P-A_y$	$D_{NN'}$
7.00	7.72	80.5	-0.157 ± 0.008	0.248 ± 0.030	0.405 ± 0.032	-0.389 ± 0.041
11.00	12.13	123.4	-0.260 ± 0.007	0.212 ± 0.026	0.472 ± 0.027	-0.238 ± 0.035
12.50	13.78	139.6	-0.311 ± 0.009	0.236 ± 0.034	0.547 ± 0.036	-0.187 ± 0.046
16.00	17.63	177.5	-0.287 ± 0.008	0.048 ± 0.033	0.335 ± 0.034	-0.352 ± 0.042
19.00	20.92	209.8	-0.309 ± 0.011	0.027 ± 0.039	0.336 ± 0.041	-0.540 ± 0.053
22.00	24.21	242.0	-0.093 ± 0.014	-0.211 ± 0.053	-0.118 ± 0.055	-0.634 ± 0.071

With this in mind, extraction of the spin-sorted peak yields for the two 1^+ states in ^{12}C began by first calculating the focal plane and FPP asymmetries described in Eqs. (16) and (14), respectively, on a channel-by-channel basis over a region of excitation energy from approximately 11 to 17 MeV. The polarization observables of the background distributions (that is, all regions of excitation energy excluding those of the narrow states) were then fitted using error-weighted cubic spline functions, as were the unpolarized total yield and FPP efficiency η_{FPP}. The three polarization observables were indeed found to vary smoothly over the 6-MeV-wide fitting range in all cases, while the FPP efficiency ''observable'' was always approximately constant with excitation energy, as one would hope. The fitted observable functions thus deduced were then inserted into Eqs. (11) and (13), and a set of background functions, different for each spin state, was generated. This procedure was used to provide background functions for both the focal plane and FPP data, for a total of six spectra at each angle.

The main advantage gained with this procedure is that one uses fits to the (high statistics) focal plane background observables, Eqs. (16), to determine much of the character of the (low statistics) FPP background. In particular, the one background function that does *not* vary smoothly with energy, I_0, can be obtained without reference to the FPP spectra. The few background functions that must be extracted from the FPP spectra (the $D_{NN'}$ and P asymmetries and η_{FPP}) are determined for all four FPP spectra simultaneously. In this way, the backgrounds for the polarimeter spectra can be constrained much more tightly than could be done using the polarimeter spectra alone.

The background-subtracted yields for the two states of interest were then used in Eqs. (14) to determine the polarization observables for each transition. The statistical uncertainty in each of these yields, δN, was taken to be

$$\delta N=(P+2B)^{1/2}, \tag{17}$$

where P is the number of counts in the (background-subtracted) peak, and B is the number of counts in the fit to the background beneath the peak. These values for δN, which represent upper bounds to the statistical uncertainties in the background subtraction, were propagated through in the usual way to calculate uncertainties in the measured observables. For this last step, we assumed the yield errors to be statistically uncorrelated; though not precisely true (due to the method used for background determination), this was shown to be an excellent approximation in a few test cases.

C. Yield extraction for ^{16}O

The technique just described, in which the focal plane and FPP background spectra are fit simultaneously, imposes physically reasonable constraints on the yield extraction procedure, and thereby on the observables deduced. Unfortunately, this technique could not be applied to the states of interest in ^{16}O, as it was not possible to determine ''smooth backgrounds'' in the sense described above for ^{12}C. Due to the higher level density near the 4^- states in ^{16}O, the tails of nearby states often interfered with the peaks of interest, despite the high resolution of the K600 spectrometer. Though some of the transitions in the region of the 4^- states have natural parity and are quite broad, many other nearby states have widths comparable to those of the 4^- states ($\Gamma\lesssim45$ keV). Under these conditions, the background observables can be expected to vary over a range of excitation energy that is comparable to the width of the strong states of interest, rendering these background functions discontinuous across the states. The yield contribution due to quasielastic scattering is also larger than that observed in ^{12}C, due to the higher excitation energies and lower particle thresholds involved.

It was therefore necessary to invoke a more complex fitting procedure for ^{16}O. In this case, we decided to fit a large number of states simultaneously, extending in excitation en-

TABLE II. Normal-component spin observables for the 1^+, $T=1$ (15.11 MeV) state in ^{12}C.

θ_{LAB}	$\theta_{\text{c.m.}}$	q (MeV/c)	A_y	P	$P-A_y$	$D_{NN'}$
7.00	7.72	81.5	0.042 ± 0.004	0.009 ± 0.013	-0.032 ± 0.014	0.008 ± 0.018
11.00	12.13	123.8	-0.010 ± 0.005	0.014 ± 0.018	0.024 ± 0.018	0.148 ± 0.023
12.50	13.79	139.9	-0.098 ± 0.008	-0.002 ± 0.028	0.096 ± 0.029	0.134 ± 0.037
16.00	17.64	177.7	-0.200 ± 0.012	-0.055 ± 0.045	0.145 ± 0.046	-0.026 ± 0.057
19.00	20.93	209.6	-0.518 ± 0.036	-0.055 ± 0.103	0.463 ± 0.110	-0.163 ± 0.139
22.00	24.22	241.6	0.026 ± 0.073	-0.024 ± 0.267	-0.049 ± 0.277	0.041 ± 0.348

TABLE III. Normal-component spin observables for the 4^-, $T=0$ (17.78 MeV) state in ^{16}O.

θ_{LAB}	$\theta_{\text{c.m.}}$	q (MeV/c)	A_y	P	$P-A_y$	$D_{NN'}$
20.50	22.07	225.5	0.146 ± 0.013	0.214 ± 0.054	0.069 ± 0.055	0.397 ± 0.071
28.00	30.11	304.6	0.142 ± 0.011	0.188 ± 0.045	0.046 ± 0.046	0.563 ± 0.059
37.00	39.70	397.4	0.072 ± 0.011	0.092 ± 0.043	0.021 ± 0.044	0.687 ± 0.058

ergy from about 16.5 to 21 MeV, i.e., from ~1 MeV below the lowest energy 4^- state to 1 MeV above the highest. To do so, we used the program [41], designed to perform line shape analyses of spectra. Prior to the actual peak fitting, though, parameters for the spin-dependent, smooth background underlying these peaks (see below) were determined by fitting the regions between peaks, imposing constraints similar to those used in the ^{12}C analysis described in the previous subsection. These background parameters were then put into ALLFIT by hand, and the fit to the data proceeded on top of these externally determined backgrounds. By simultaneously fitting the peaks for all of the transitions of interest, as well as for all nearby states, we were able to determine the spin-dependent, raw yields for each of the three 4^- states. This fitting procedure had to be applied separately to each of the six ''spin-sorted'' spectra, as the version of ALLFIT we used could fit only one spectrum (and thus only one spin state) at a time.

In determining the background parameters, it was assumed that most of the ''smooth'' features were due to quasielastic nucleon knockout reactions, which set in above particle threshold. This suggested we use a function that was approximately constant but slowly rising at higher excitation energies, and had an abrupt turn on at threshold. This general shape is apparent in Fig. 5. Because these data were obtained with ^{10}B-enriched H_3BO_3 targets, spectra from pure ^{10}B were required to isolate continuum contributions from each nucleus. After suitable subtraction, a parameterized function was obtained which reproduced the underlying continuum fairly well. This background function, which is shown in Fig. 5, is given by

$$\begin{aligned} \text{bkgd}&=0; \quad E_{ex}<E_1, \\ &=a(E_{ex}-E_1)^{1/2}; \quad E_1<E_{ex}<E_2, \\ &=a[(E_{ex}-E_1)^{1/2}+(E_{ex}-E_2)^{1/2}], \quad E_2<E_{ex}, \end{aligned} \tag{18}$$

where a is an empirically adjusted normalization parameter and E_1 (=12.1 MeV) and E_2 (=15.7 MeV) are the proton and neutron threshold energies, respectively. From Fig. 5 one can see that this function is approximately linear over the range of interest in ^{16}O, so that two peak-free ranges at the low and high excitation ends of the spectra were sufficient to determine all needed background parameters. After the high-statistics focal plane spectra had been thus analyzed, the backgrounds of the four FPP spectra were determined using the same ranges, but constrained in a manner similar to that used for the ^{12}C analysis.

An asymmetric Gaussian line shape was used for all peaks in each spectrum. To begin the analysis, the shape-defining peak parameters were first adjusted for each run in order to reproduce the spectrometer response to a strong, isolated peak, such as a low-lying natural-parity state or, if possible, to the elastic scattering peak. With these peakshape parameters and those of the (previously deduced) background held fixed, the fitting would proceed by initially including peaks for all known ^{16}O states between 16.4 and 21 MeV of excitation. (Data taken separately on thin, pressed ^{10}B targets indicated that there are no strongly excited states in this nucleus over this energy range.) In the fitting procedure, only the peak amplitudes were allowed to vary; for each state, its position (excitation energy) was fixed at its nominal value [40], while its width was determined by adding in quadrature the intrinsic width quoted in the data tables [40] with the measured resolution of the spectrometer. This latter quantity was taken to be the width observed for the narrowest state in the spectrum, the 4^- state at 18.977 MeV ($\Gamma=8\pm4$ keV, well below the experimental resolution).

In subsequent iterations, the amplitudes of all peaks, as well as the widths and centroids of the three 4^- states, were allowed to vary. In all cases, the fitted centroids for the 4^- states corresponded, within statistical error, to their quoted excitation energies [40]. In a few instances, when the data showed a peak that was cleanly resolved from the rest of the spectrum, the width of that peak was also allowed to vary along with its height. However, for the majority of the states, which were generally weak and overlapping with other states, the data did not sufficiently constrain the fit, and the centroids and effective widths (as described above) were held fixed. Once a suitable fit had been obtained to the data in the high statistics spectrum, the same parameters were used in fits to the six spin-sorted spectra, and only the peak amplitudes were allowed to vary. The statistical uncertainties in the yields obtained using this technique are from the error matrix in ALLFIT, and include the statistical, but not any systematic, uncertainties in the background determination.

With the spin-sorted yields in hand, it was then straightforward to use Eqs. (14) to generate our final values for the observables. These are presented in Tables I–V and Figs. 6–10 for the five excited states of interest in this work. In these tables, and in all the figures that follow, the errors shown include contributions from both statistical and systematic uncertainties. The former dominate in all cases for the observables P, $P-A_y$, and $D_{NN'}$, while the errors for A_y are predominantly due to uncertainties in the precise magnitude of the beam polarization.

V. RESULTS AND DISCUSSION

A. Theoretical calculations

Though the main purpose of this paper is the presentation of our measured values for the normal-component spin ob-

TABLE IV. Normal-component spin observables for the 4^-, $T=1$ (18.98 MeV) state in ^{16}O.

θ_{LAB}	$\theta_{\text{c.m.}}$	q (MeV/c)	A_y	P	$P-A_y$	$D_{NN'}$
20.50	22.08	225.5	0.225 ± 0.007	0.258 ± 0.029	0.034 ± 0.030	0.021 ± 0.038
28.00	30.11	304.3	0.291 ± 0.008	0.250 ± 0.033	-0.040 ± 0.034	-0.079 ± 0.043
37.00	39.71	396.9	0.416 ± 0.014	0.346 ± 0.055	-0.070 ± 0.057	-0.079 ± 0.072

servables, much can be learned by comparing our results to the predictions of state-of-the-art theoretical models. All calculations shown here were carried out in the distorted wave impulse approximation (DWIA) using the computer code [42]. We first describe the various components that serve as input to these calculations.

A fairly good description of spin-flip transitions [17] has been obtained using the density-dependent DBHF (Dirac-Brueckner Hartree-Fock) interaction of Sammarruca and Stephenson [43,17]. This interaction starts with a one-boson-exchange NN potential (an updated version of the Bonn-B potential [44]) that provides an excellent fit to the current NN database below pion threshold [45]. By solving the Bethe-Goldstone equation in infinite nuclear matter, a density-dependent effective interaction is obtained that includes effects due to Pauli blocking, nuclear binding, and relativistic corrections that arise from the large (and partially canceling) scalar and vector nuclear mean fields. The G matrix thus produced is converted to a Yukawa function representation, and can then be inserted into the DWIA code. The DBHF calculations were run using DWBA86, as this program allows for finite range DWIA for the exchange contributions. This is an important concern for an accurate description of spin-flip transitions.

For both nuclei, the incoming and outgoing wave distortions were calculated using a folding model potential. Using the parameterized charge density for each nucleus [46], and assuming equal proton and neutron distributions for these $N=Z$ nuclei, the central and spin-orbit interaction terms were averaged over the target nucleon distributions. This same distribution also yielded the local density at which the effective NN interaction was evaluated. In this sense, use of a $t\rho$ approximation for the optical potential means that the distortions are calculated ''self-consistently,'' in that the same amplitudes used in the impulse approximation to drive the transition are also used to distort the nucleon waves. However, prior work suggests [47] that relativistic medium effects are weaker in the elastic channel than in the effective interaction that drives (p,p') inelastic scattering, and better agreement with measurements of elastic scattering data can be obtained by using that portion of the model that incorporates only Pauli blocking and nuclear binding effects. Therefore, for comparisons between our data and this effective interaction, we have chosen to include only these nonrelativistic medium modifications in our $t\rho$ approximation for the distorted waves.

As discussed in Sec. I, the transition form factors for each of the three strong 4^- states in ^{16}O can be well described by a single $d_{5/2}p_{3/2}^{-1}$ ''stretched'' particle-hole configuration. The particle and hole wave functions are treated as states in a standard Woods-Saxon well, rather than using a harmonic oscillator potential, using the ansatz discussed in Ref. [17] to obtain the well parameters. These parameters, and the spectroscopic factors, were adjusted in order to reproduce the transverse form factors measured in the inelastic (e,e') studies of Hyde-Wright [24]. This procedure provides a tight constraint for the $T=1$ state, a weaker constraint on the lower $T=0$ state, and little information for the upper isoscalar state [17], due to the isospin mixing of these states. The isospin composition of these states had been previously determined using measured strength asymmetries between π^+ and π^- inelastic scattering [25]. The pion cross sections and angular distributions were calculated in a DWIA assuming a simple three-state mixing model, with the relative isospin-mixing amplitudes adjusted [26] to provide the best fit to the data. These results suggest that the strong state observed at 18.98 MeV is almost pure isovector, while the states at 17.79 and 19.80 MeV are predominantly $T=0$, but contain small ($\sim$20%) $T=1$ amplitude admixtures of comparable size but opposite sign.

Due to the insensitivity of inelastic electron scattering to $\Delta S=1$ isoscalar transitions, the nuclear structure for the $T=0$ state at 12.71 MeV in ^{12}C is not as well determined as that of the 15.11 MeV, $T=1$ state. In particular, the overall magnitude of the isoscalar transition form factor is relatively unconstrained, which compromises the information contained in the polarized cross sections to be discussed below. In addition, for lower spin, unnatural-parity states such as these, there are many particle-hole combinations that can contribute to the structure, and electron or pion scattering is of limited value in sorting out the relative amplitudes for each. Because spin observables are sensitive to the choice of amplitudes, one must be guided by model calculations,

TABLE V. Normal-component spin observables for the 4^-, $T=0$ (19.81 MeV) state in ^{16}O.

θ_{LAB}	$\theta_{\text{c.m.}}$	q (MeV/c)	A_y	P	$P-A_y$	$D_{NN'}$
20.50	22.08	225.4	0.239 ± 0.011	0.332 ± 0.045	0.093 ± 0.047	0.647 ± 0.060
28.00	30.12	304.2	0.204 ± 0.009	0.339 ± 0.040	0.135 ± 0.041	0.785 ± 0.054
37.00	39.71	396.5	0.047 ± 0.009	0.078 ± 0.037	0.032 ± 0.038	0.802 ± 0.051

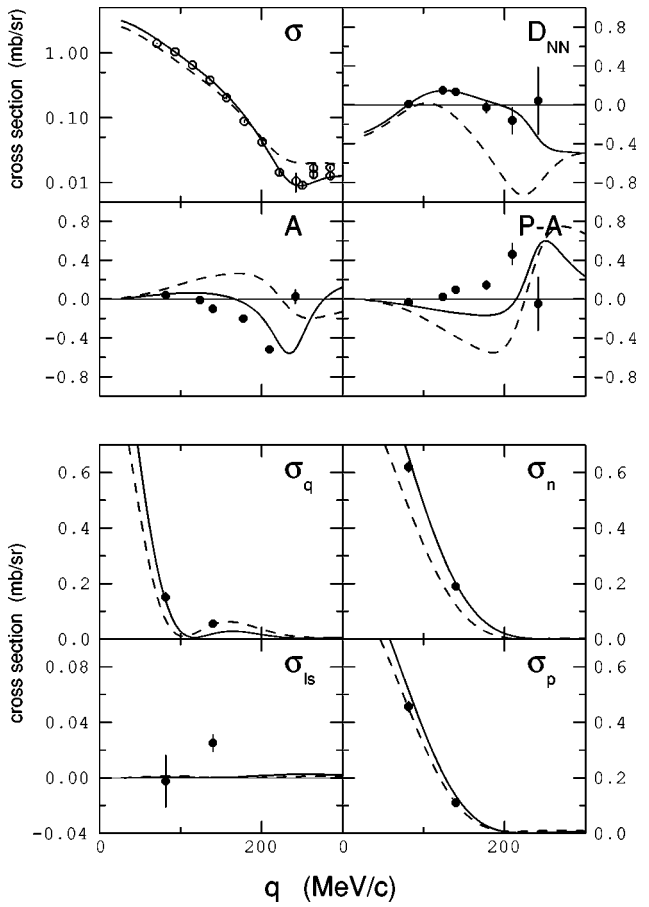

FIG. 6. Differential cross section, normal-component spin observables, and polarized cross sections for the isovector 1^+ state at 15.11 MeV in ^{12}C. The solid lines are DWIA calculations using the DBHF interaction of Sammarruca and Stephenson [43], while the dashed lines use the free interaction of the same group.

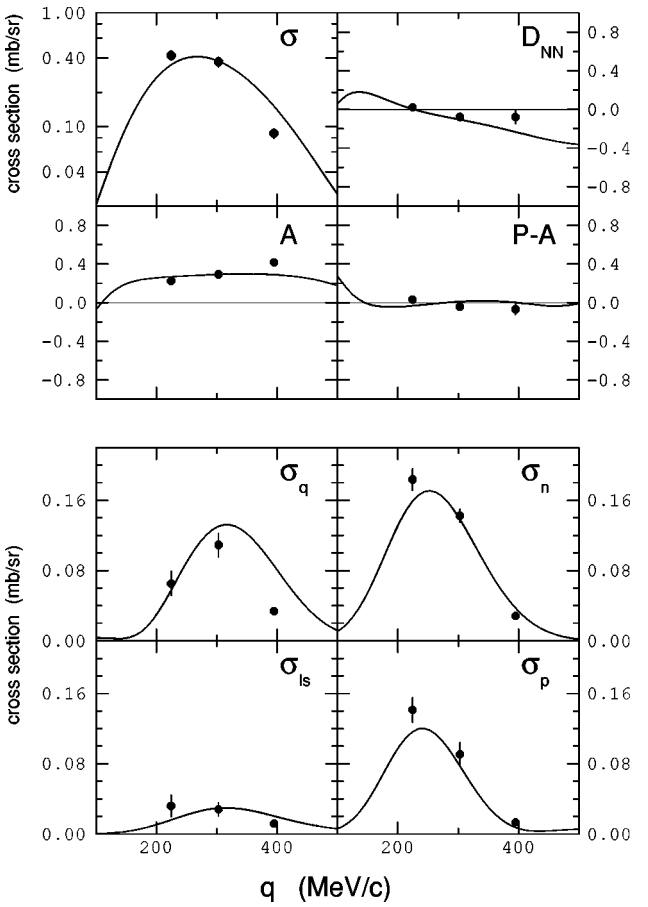

FIG. 7. Same as Fig. 6, but for the isovector 4^- state at 18.98 MeV in ^{16}0. The free interaction predictions are not shown.

which introduces a significant ambiguity into the interpretation of these data. For this work, predictions for the 1^+ $T=0$ transition used Cohen-Kurath amplitudes for the nuclear wave functions [48], which include particle-hole amplitudes only for the $p_{3/2}$ and $p_{1/2}$ shells. For the $T=1$ state, more current amplitudes were obtained from Millener, who provided an improved version of the particle-hole matrix elements found in Table I of Ref. [49]. It is important to point out that the amplitudes used are clearly invalid beyond momentum transfers of $q\sim225$ MeV/c for the $T=0$ state, and ~300 MeV/c for the $T=1$, at which point the predicted cross sections start to fall well below the data [50], as can be seen in the upper left panels of Figs. 8 and 6, respectively.

B. Discussion of the observables

The values obtained in this work for $D_{NN'}$ for the two isovector transitions are shown in the upper panels of Figs. 6 and 7, along with the DBHF predictions described above. The $D_{NN'}$ data for both of these states are fairly close to zero over the entire range of momentum transfer covered by this experiment, indicating that the normal component of the scattered polarization is largely independent of the normal component of the incident beam. The DBHF calculation (solid line) for the 15.11 MeV state in ^{12}C (Fig. 6) follows the data very well, which is a considerable success for this interaction, given earlier problems encountered in reproducing this observable [9,20,34]. The calculated effects of the nuclear medium, indicated by the differences between the two curves, are often quite large, and are clearly important to include for comparisons with data at this level of precision. The cross section [50] is also reproduced very well, at least over the first lobe. The situation is similar for the 18.98 MeV state in ^{16}O, though the $D_{NN'}$ calculation exhibits a stronger slope than is seen in the data. We return to this point in the next section. For all of the 4^- state calculations, the free interaction curves are not shown, as they are largely indistinguishable from the medium-modified DBHF curves. This is to be expected for stretched states, whose high angular momentum components lead to very surface-peaked transition wave functions.

Figures 8–10 show the data and calculations for the isoscalar transitions in ^{12}C and ^{16}O. For the 12.71 MeV state in ^{12}C, there are clearly problems: the cross section is underpredicted and starts to deviate in shape from the data at fairly small values of momentum transfer. The q dependence of $D_{NN'}$, on the other hand, is well described by the DBHF calculation, but appears slightly more negative. Though not shown, we mention that use of a similar BHF interaction, i.e., one in which first-order relativistic effects have *not* been

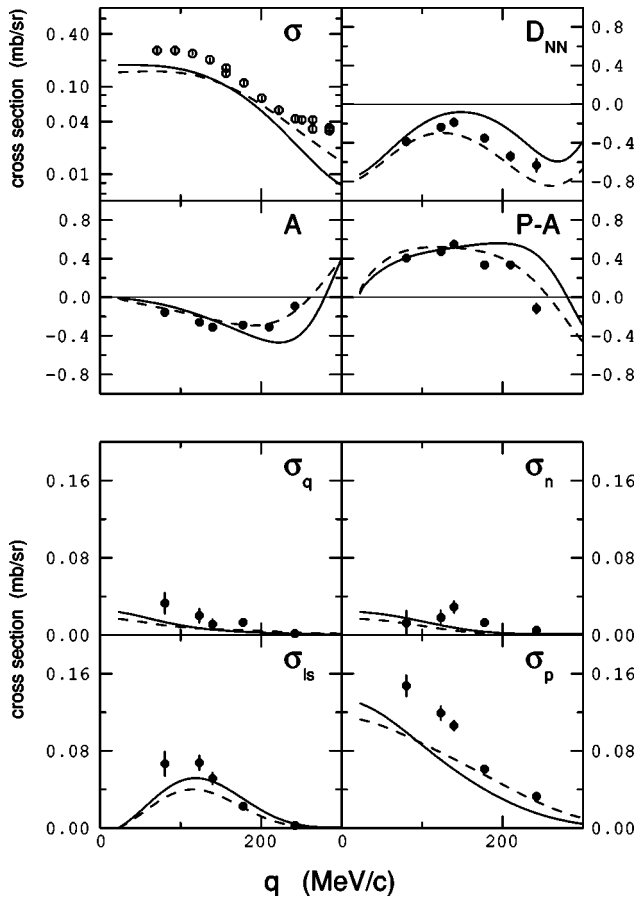

FIG. 8. Same as Fig. 6, but for the isoscalar 1^+ state at 12.71 MeV in ^{12}C.

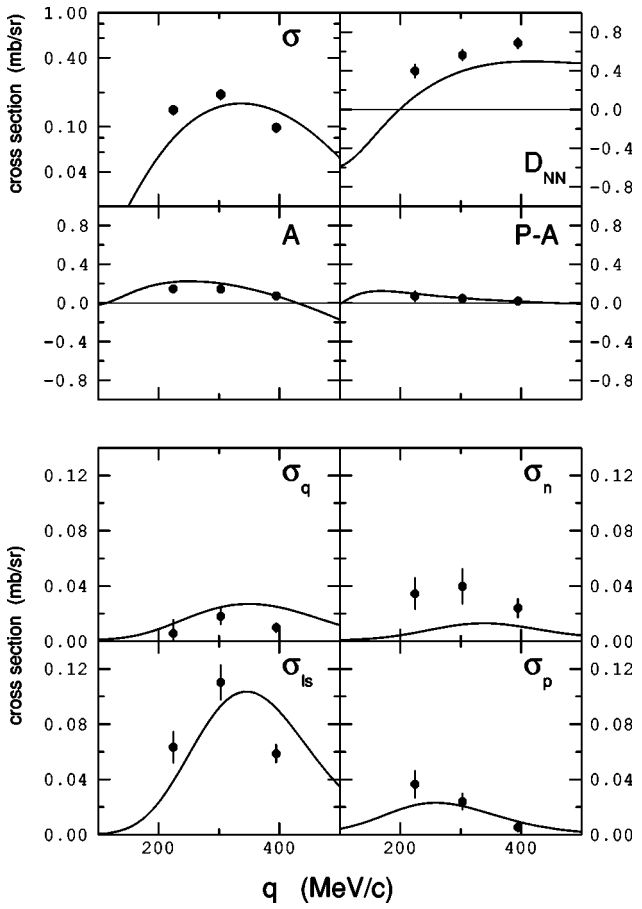

FIG. 9. Same as Fig. 6, but for the isoscalar 4^- state at 17.78 MeV in ^{16}0.

included, leads to almost perfect agreement with the data for $D_{NN'}$. This may be related to the concern discussed above in reference to use of the DBHF interaction to generate the distorting potential; the resulting potential appears to be too repulsive in the nuclear interior. This sort of problem would tend to affect low spin transitions, e.g., 1^+ states, much more severely than high spin, surface-peaked transitions. For the isoscalar 4^- states in ^{16}O (Figs. 9 and 10), DWIA calculations using DBHF reproduce the general shape of $D_{NN'}$ fairly well, though are again somewhat off in overall magnitude, more so for the lower (17.78 MeV) than the upper (19.81 MeV) state. This discrepancy is indicative of a larger problem with the isoscalar interaction, as evidenced by the inability of these calculations to predict the peak location of the cross sections for these states. The source of this problem will be discussed below, once polarized cross sections have been introduced.

As pointed out earlier, nonzero values of $(P-A_y)$ can be attributed to the presence of nonlocalities in the effective NN interaction. However, Moss has shown [6] that for unnatural parity transitions in which a single combination of $[LSJ]$ dominates (as is true for the stretched 4^- states in ^{16}O), $(P-A_y)$ will also vanish due to its structure. With a few simplifying assumptions, Love has independently demonstrated [10] that for stretched states neither the convection current nor spin terms contribute; thus the composite spin current terms, which will generally make nonzero contributions to $(P-A_y)$, vanish. These arguments are borne out in Figs. 7, 9, and 10, in which both data and calculations show $(P-A_y)$ always close to zero for the 4^- states in ^{16}O. This is true despite the nonzero values observed for P and A_y separately, which are both predicted quite well by the DBHF calculations for all three states.

The situation is somewhat different for the ^{12}C 1^+ states, where the calculations have a more difficult time reproducing the single-spin asymmetries P and A_y. For the isoscalar state (Fig. 8), A_y is predicted reasonably well, though only for values of momentum transfer up to $q\sim250$ MeV/c, beyond which data and predictions diverge wildly. The basic shape of the difference function $(P-A_y)$ is also reproduced, though it appears to be shifted slightly in q. We will attempt to sort out these shortcomings of the isoscalar interaction below. The real puzzle, however, is the isovector state, shown in Fig. 6. In this case, we are reasonably confident that the effective interaction is under control [17]. Based on the comparisons of calculations and data for the remaining observables, one might also conclude that the structure of this transition is well described by the amplitudes of Millener [49]. Viewed in this context, it is very surprising that the difference function $(P-A_y)$ is reproduced so poorly, due largely to the inability of the calculation to follow the induced polarization P. Historically, this long-standing prob-

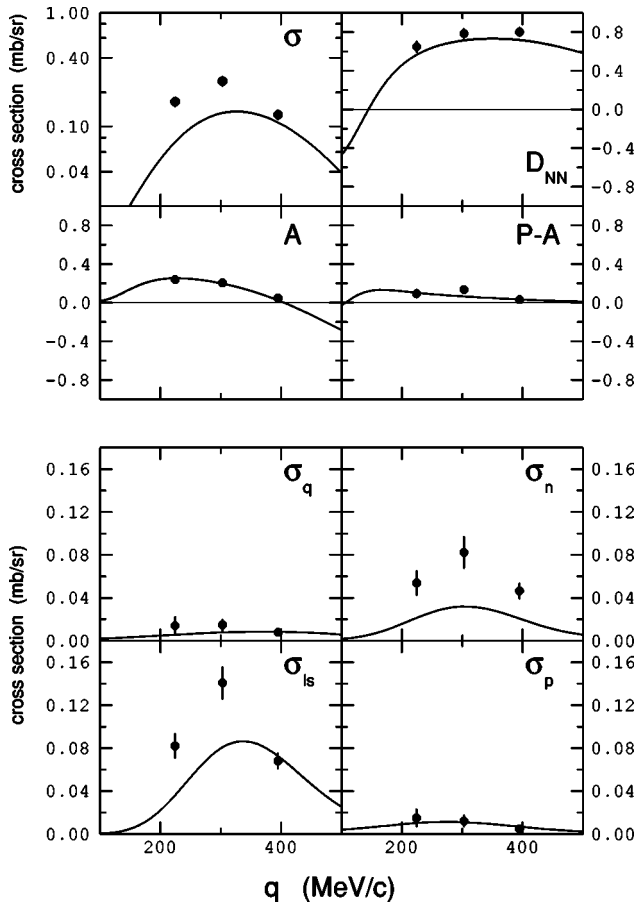

FIG. 10. Same as Fig. 6, but for the isoscalar 4^- state at 19.81 MeV in ^{16}0.

lem has been dismissed as a simple structure problem [21]. However, because the nuclear currents which give rise to $(P-A_y)$ are the result (at least nonrelativistically) of exchange processes [14], which sample the effective interaction at momentum transfers much larger than those relevant for the direct process, this discrepancy might also suggest that the isovector interaction does require some modification, at very high q values, in order to reproduce the data.

C. Polarized cross sections

To fully exploit the information contained in these spin observables, one would like to establish a more direct connection between the measured data sets and the individual terms of the *NN* interaction as parametrized, for example, in Eq. (2). To do so requires that one has access to the complete spin-transfer matrix, which contains eight nonvanishing coefficients [8]. For the five transitions discussed here, such matrices do exist when the present data set, consisting of the normal-component spin observables, are combined with the in-plane measurements of Olmer *et al.* [16]. With these complete data sets in hand, it is useful to define the following combinations of observables:

$$D_{ls} \equiv [1 + D_{NN'} + (D_{SS'} + D_{LL'})\cos\theta - \delta \sin\theta]/4,$$

$$D_q \equiv [1 - D_{NN'} + D_{SS'} - D_{LL'}]/4,$$

$$D_n \equiv [1 + D_{NN'} - (D_{SS'} + D_{LL'})\cos\theta + \delta \sin\theta]/4,$$

$$D_p \equiv [1 - D_{NN'} - D_{SS'} + D_{LL'}]/4, \tag{19}$$

where θ is the center of mass scattering angle and $\delta \equiv D_{LS'} - D_{SL'}$. It has been pointed out by several authors [6,7] that with a few simplifying assumptions (e.g., neglecting distortions), these particular combinations of observables can be related to specific amplitudes of the effective interaction via

$$\sigma_{ls} \equiv \sigma D_{ls} = C^2 \chi_T^2, \quad \sigma_q \equiv \sigma D_q = E^2 \chi_L^2,$$

$$\sigma_n \equiv \sigma D_n = B^2 \chi_T^2, \quad \sigma_p \equiv \sigma D_p = D^2 \chi_T^2. \tag{20}$$

In the above expressions, χ_T (χ_L) is the spin transverse (longitudinal) form factor, and σ is the differential cross section. Note that by studying transitions to discrete states such as these, *all* of the spin-dependent KMT amplitudes can be probed, rather than just the two combinations available, for example, in quasielastic measurements [2–5].

The experimental values for the polarized cross sections $\sigma_\lambda \equiv \sigma D_\lambda$, with D_λ defined in Eq. (19), are presented in the bottom halves of Figs. 6–10 for each of the five transitions. Turning to the isovector states first, it is not too surprising, in light of the preceding discussion, that the DBHF calculations work very well for both the ^{12}C and ^{16}O states. As expected on general grounds [51], the polarized cross section σ_{ls}, driven primarily by the strength of the spin-orbit amplitude, is indeed found to be very small, especially in the low-q regime probed by the 1^+ state. The division of strength among the three tensor components is also seen to be about right over most of the range of momentum transfer studied here, though some small amount of fine-tuning may be required near 200 MeV/c. The only real discrepancy arises at the very highest values of q, where the predicted magnitude of σ_q is clearly far too strong, reflecting most of the overestimate seen in the differential cross section for the ^{16}O isovector 4^- state. This may have some bearing on the problems noted above with regard to exchange processes and an inability to predict the observable $(P-A_y)$. Overall, though, the ability of the DBHF interaction to reproduce essentially all features of the isovector amplitudes is remarkably good, and must be viewed as a major success of this OBE *NN* interaction and the medium modifications imposed on it.

For the isoscalar interaction, on the other hand, significant problems remain. In this isospin channel, the spin-orbit amplitude is dominant, and appears to be of approximately the right magnitude for both the ^{12}C and ^{16}O states. A simple interpretation is rendered more difficult, though, due to the mismatch seen between the predicted and measured cross sections for these states. For the 4^- state in ^{16}O at 17.78 MeV, for example (Fig. 9), the predicted values for both σ and σ_{ls} deviate from the data in a very similar pattern. This is, in large part, a result of an overestimate of the size of the isoscalar spin-orbit component of the effective interaction at large momentum transfer when medium effects are included, and arises from the part of the calculation that treats Pauli blocking and nuclear binding in infinite nuclear matter. By

making the amplitude C of Eqs. (2) and (20) too large at high q, the result is to push the peak in σ_{ls}, and hence σ, out to larger angles.

While the spin-orbit strength appears to be about right (albeit with an incorrect q dependence), the tensor amplitudes calculated in DBHF are in general too weak in the isoscalar channel, though some of this may simply reflect the uncertainty in the magnitude of the transition form factor. The polarized cross section data for σ_n are relatively small, but the predictions for this quantity are smaller yet, by roughly a factor of 2. Similarly, the calculated values for σ_p consistently fall below the data at all but the largest momentum transfers. Unfortunately, while complete data sets such as these can help to pinpoint problems, they provide little guidance as to the underlying source of these discrepancies. One concern, though, becomes apparent in a detailed examination of the one-boson-exchange model itself at the energies and momentum transfers being examined here. For the isoscalar tensor amplitudes, the direct component is due primarily to the exchange of ω and η mesons, whose contributions largely cancel for the choice of coupling constants employed in the model [17]. The tensor exchange is also driven by canceling mesons, in this case between the attractive π term and the equally repulsive ρ, when evaluated at the relevant momentum transfers of $q \sim 600$ MeV/c. These cancelations tend to keep the tensor strength weak, but also make the calculations highly sensitive to even small changes in the contributions of the various mesons, such as those produced by the presence of the nuclear medium. Some preliminary studies of several possible sources of these types of effects have already been carried out [17].

VI. SUMMARY AND CONCLUSIONS

To exploit the increased sensitivity predicted for polarization observables to the spin-dependent terms of the effective NN interaction, we have made high precision measurements of the normal-component polarization observables $D_{NN'}$, P, and A_y for the inelastic scattering of 198 MeV protons from five unnatural-parity states in light nuclei. These transitions are the two dominant 1^+ states in ^{12}C at 12.71 MeV ($T=0$) and 15.11 MeV ($T=1$), and the three 4^- stretched states in ^{16}O at 17.78 and 19.81 MeV ($T=0$) and 18.98 MeV ($T=1$). These data, when combined with previously measured in-plane observables, provide complete sets of spin transfer observables for all five of these transitions, and specific linear combinations of observables have been formed which can isolate individual terms of the effective NN interaction.

The new data, as well as these combinations of observables, have been compared with a distorted wave impulse approximation calculation in which the nuclear medium has been treated microscopically in order to yield an effective NN interaction which accounts for Pauli blocking, nuclear binding, and relativistic corrections. The comparisons indicate that the isovector interaction is predicted very well, with problems arising only at the very largest values of momentum transfer, i.e., those relevant for tensor exchange contributions. In the isoscalar channel, large differences between data and theory show that the net effect of the medium modifications has been to shift the dominant spin-orbit amplitude towards larger values of q in the calculation than the data require, and that the tensor strengths, while quite weak, are predicted to be even weaker. These data should continue to provide important and stringent tests as new and more complete models of the effective NN interaction are developed.

ACKNOWLEDGMENTS

The authors would like to thank D. J. Millener for providing the particle-hole matrix elements used for the 1^+, $T=1$ transition in ^{12}C. This work was supported by the U.S. National Science Foundation through Grant No. NSF-PHY-9602872.

[1] W. Glöckle, H. Witała, D. Hüber, H. Kamada, and J. Golak, Phys. Rep. **274**, 107 (1996).
[2] L. B. Rees *et al.*, Phys. Rev. C **34**, 627 (1986).
[3] O. Häusser *et al.*, Phys. Rev. C **43**, 230 (1991).
[4] T. N. Taddeucci *et al.*, Phys. Rev. Lett. **73**, 3516 (1994).
[5] T. Wakasa *et al.*, Phys. Rev. C **59**, 3177 (1999).
[6] J. M. Moss, Phys. Rev. C **26**, 727 (1982).
[7] E. Bleszynski, M. Bleszynski, and C. A. Whitten, Jr., Phys. Rev. C **26**, 2063 (1982).
[8] G. G. Ohlsen, Rep. Prog. Phys. **35**, 717 (1972).
[9] S. Seestrom-Morris *et al.*, Phys. Rev. C **26**, 2131 (1982).
[10] W. G. Love, in *Spin Excitations in Nuclei*, edited by F. Petrovich, G. E. Brown, G. T. Garvey, C. D. Goodman, R. A. Lindgren, and W. G. Love (Plenum, New York, 1984), p. 205.
[11] D. A. Sparrow *et al.*, Phys. Rev. Lett. **54**, 2207 (1985).
[12] R. D. Amado, Phys. Rev. C **26**, 270 (1982).
[13] J. Piekarewicz, R. D. Amado, and D. A. Sparrow, Phys. Rev. C **32**, 949 (1985).
[14] W. G. Love and J. R. Comfort, Phys. Rev. C **29**, 2135 (1984).
[15] E. Rost and J. R. Shepard, Phys. Rev. C **35**, 681 (1987).
[16] C. Olmer, in *Antinucleon- and Nucleon-Nucleus Interactions*, edited by G. E. Walker, C. D. Goodman, and C. Olmer (Plenum, New York, 1985), p. 261.
[17] F. Sammarruca, E. J. Stephenson, K. Jiang, J. Liu, C. Olmer, A. K. Opper, and S. W. Wissink, Phys. Rev. C **61**, 014309 (2000).
[18] J. B. McClelland *et al.*, Phys. Rev. Lett. **52**, 98 (1984).
[19] X. Y. Chen, J. R. Shepard, M. R. Braunstein, T. A. Carey, K. W. Jones, J. B. McClelland, L. Rees, T. N. Taddeucci, N. Tanaka, and A. D. Bacher, Phys. Rev. C **44**, 2041 (1991).
[20] S. P. Wells *et al.*, Phys. Rev. C **52**, 2559 (1995); S. P. Wells and S. W. Wissink, *ibid.* **61**, 014601 (2000).
[21] T. A. Carey *et al.*, Phys. Rev. Lett. **49**, 266 (1982).
[22] K. H. Hicks *et al.*, Phys. Lett. B **201**, 29 (1988).
[23] R. A. Lindgren and F. Petrovich, in *Spin Excitations in Nuclei*, edited by F. Petrovich, G. E. Brown, G. T. Garvey, C. D. Goodman, R. A. Lindgren, and W. G. Love (Plenum, New York, 1984), p. 323.

[24] C. E. Hyde-Wright *et al.*, Phys. Rev. C **35**, 880 (1987).
[25] D. B. Holtcamp *et al.*, Phys. Rev. Lett. **45**, 420 (1980).
[26] J. A. Carr, F. Petrovich, D. Halderson, D. B. Holtkamp, and W. B. Cottingham, Phys. Rev. C **27**, 1636 (1983).
[27] B. Larsen *et al.*, Phys. Rev. C **53**, 1774 (1996).
[28] E. Donoghue *et al.*, Phys. Rev. C **43**, 213 (1991).
[29] H. Baghaei *et al.*, Phys. Rev. Lett. **69**, 2054 (1992).
[30] Jian Liu, E. J. Stephenson, A. D. Bacher, S. M. Bowyer, S. Chang, C. Olmer, S. P. Wells, S. W. Wissink, and J. Lisantti, Phys. Rev. C **53**, 1711 (1996); E. J. Stephenson, J. Liu, A. D. Bacher, S. M. Bowyer, S. Chang, C. Olmer, S. P. Wells, S. W. Wissink, and J. Lisantti, Phys. Rev. Lett. **78**, 1636 (1997).
[31] A. K. Kerman, H. McManus, and R. M. Thaler, Ann. Phys. (N.Y.) **8**, 551 (1959).
[32] L. Wolfenstein, Annu. Rev. Nucl. Sci. **6**, 43 (1956).
[33] G. P. A. Berg *et al.*, IUCF Scientific and Technical Report 1986, p. 152.
[34] A. K. Opper, Ph.D. thesis, Indiana University, 1991.
[35] See, for example, W. Haeberli, Annu. Rev. Nucl. Sci. **17**, 373 (1967).
[36] E. J. Stephenson, A. D. Bacher, G. P. A. Berg, V. R. Cupps, C. C. Foster, N. Hodiwalla, P. Li, J. Lisantti, D. A. Low, D. W. Miller, C. Olmer, A. K. Opper, B. K. Park, R. Sawafta, S. W. Wissink, J. A. Tostevin, D. A. Coley, and R. C. Johnson, Phys. Rev. C **42**, 2562 (1990).
[37] LeCroy Research Corporation, 700 Chestnut Ridge Road, Chestnut Ridge, NY 10977.
[38] M. W. McNaughton *et al.*, Nucl. Instrum. Methods Phys. Res. A **241**, 435 (1985), and references therein.
[39] E. Aprile-Giboni *et al.*, Nucl. Instrum. Methods Phys. Res. **215**, 147 (1983), and references therein.
[40] F. Ajzenberg-Selove, Nucl. Phys. **A506**, 1 (1990); D. R. Tilley, H. R. Weller, and C. M. Cheves, *ibid.* **A564**, 1 (1993).
[41] J. J. Kelly, program ALLFIT (unpublished).
[42] R. Schaeffer and J. Raynal, program DWBA, Saclay Report No. CEA–R4000, 1970; modifications by S. M. Austin, W. G. Love, J. R. Comfort, and C. Olmer (private communication).
[43] F. Sammarruca, E. J. Stephenson, and K. Jiang, Phys. Rev. C **60**, 064610 (1999).
[44] R. Machleidt, Adv. Nucl. Phys. **19**, 189 (1989).
[45] V. G. J. Stoks *et al.*, Phys. Rev. C **48**, 792 (1993).
[46] H. de Vries, C. W. de Jager, and C. de Vries, At. Data Nucl. Data Tables **36**, 495 (1987).
[47] R. J. Furnstahl and S. J. Wallace, Phys. Rev. C **47**, 2812 (1993).
[48] S. Cohen and D. Kurath, Nucl. Phys. **A101**, 1 (1967); T. H. S. Lee and D. Kurath, Phys. Rev. C **21**, 293 (1980).
[49] F. P. Brady *et al.*, Phys. Rev. C **43**, 2284 (1991); D. J. Millener (private communication).
[50] J. R. Comfort, R. E. Segel, G. L. Moake, D. W. Miller, and W. G. Love, Phys. Rev. C **23**, 1858 (1981).
[51] W. G. Love and M. A. Franey, Phys. Rev. C **24**, 1073 (1981).